Intense THz Generation with New Organic NLO Crystal NMBA

Daisy J.H. Ludlow, Bruce Wayne H. Palmer, Natalie K. Green, Sin-Hang Enoch Ho, Coriantumr Z. Wayment, Brenan M. Kelleher, Connor D. Barlow, Olivia N. Rollans, Brittan P. Hunter, Claire Rader, Matthew J. Lutz, Tanner Manwaring, Stacey J. Smith, David J. Michaelis,* and Jeremy A. Johnson*

Large crystal growth and characterization of the optical and terahertz (THz) properties of organic nonlinear optical (NLO) crystal NMBA (4-Nitro-4′-methylbenzylidene aniline) is presented. The reported method of crystal growth consistently produces high-quality single crystals. The THz generation efficiency and optical properties of NMBA to other THz generation crystals including BNA and MNA are compared. The low THz absorptions that make NMBA an ideal source for THz time-domain spectroscopy are highlighted.

1. Introduction

Optical rectification of near infrared light using organic nonlinear optical (NLO) crystals is one of the most widely used generation sources of terahertz (THz) frequencies of light. Organic NLO crystals have high conversion efficiencies that lead to strong single-cycle electric fields with broad bandwidths from 0.5 to 10 THz. An ideal broadband THz generator should have low absorptions across a range of generated frequencies, producing a smooth spectrum[1] Broad, smooth spectra are especially important for THz transmission measurements, where strong absorptions of THz frequencies in the generation crystal reduce spectral amplitude in the generated THz. Lower amplitudes translate into reduced information about the sample at those frequencies. A crystal with low absorptions across the range of THz frequencies will also have a smooth THz refractive index, which can facilitate phase-matching. If the group index at the pump wavelength closely matches the refractive indices of THz frequencies, there is less destructive interference and more amplification of the THz. Low values in the absorption coefficient correspond to smaller steps in the real part of the refractive index. If the steps are smaller, then the refractive index is more constant across the range of frequencies, allowing pump wavelengths to be well phase-matched with the entire range of generated THz. Good phase matching across the whole range of THz frequencies leads to generation of broad, smooth spectra, which are optimized for spectroscopic application. Crystals such as DAST and OH1 have peaks in their absorption coefficients that exceed 500 cm^{-1}, giving these crystals strong absorptions and dips in refractive index in the 0–6 THz range. Yellow crystals MNA and BNA have more broadband THz spectra because the maximum peaks in their absorption coefficient are ≈200 cm^{-1} or less.

Yellow-colored organic NLO crystals are important because they are well phase-matched with shorter NIR wavelengths, like 800 nm or 1030 nm. Red crystals such as OH1,[2] DAST,[3–6] and PNPA[7] experience strong two-photon absorption and lower damage thresholds at these shorter wavelengths, and are therefore less desirable when using 800 nm pump light. Some yellow crystals previously synthesized by our group and others include BNA,[8–10] MNA,[11] diphenylfluorenone (DPFO),[12] and OHP-CBS.[13] While the discovery and synthesis of new materials can be costly and time-consuming, we recently described a data mining approach combined with 1st-principles calculations that identify known materials in crystallographic databases that could serve as efficient THz generators. Using this method, we discovered and characterized a number of new organic THz generation crystals that exceed the performance of industry standards.[14]

From this data mining approach, we identified NMBA (4-Nitro-4′-methylbenzylidene aniline) as a high-performing yellow THz generation crystal.[14] However, a complete characterization of NMBA properties has not been reported. **Figure 1** shows a THz electric field trace of NMBA with the corresponding Fourier transform. The inset in Figure 1a highlights the high crystal quality that we achieve with our newly optimized method of synthesis and crystal growth. The inset of Figure 1b shows the broadband nature of THz generated from NMBA. In this work, we describe the synthesis and growth methods of high-quality NMBA crystals[15] and we present the optical and THz properties of these crystals. We also compare our NMBA crystals to other yellow organic NLO crystals, including BNA and MNA. We then highlight the low THz absorption features that make NMBA an ideal

D. J. Ludlow, B. W. H. Palmer, N. K. Green, S.-H. E. Ho, C. Z. Wayment, B. M. Kelleher, C. D. Barlow, O. N. Rollans, B. P. Hunter, C. Rader, M. J. Lutz, T. Manwaring, S. J. Smith, D. J. Michaelis, J. A. Johnson
Department of Chemistry and Biochemistry
Brigham Young University
Provo, UT 84604, USA
E-mail: dmichaelis@chem.byu.edu; jjohnson@chem.byu.edu
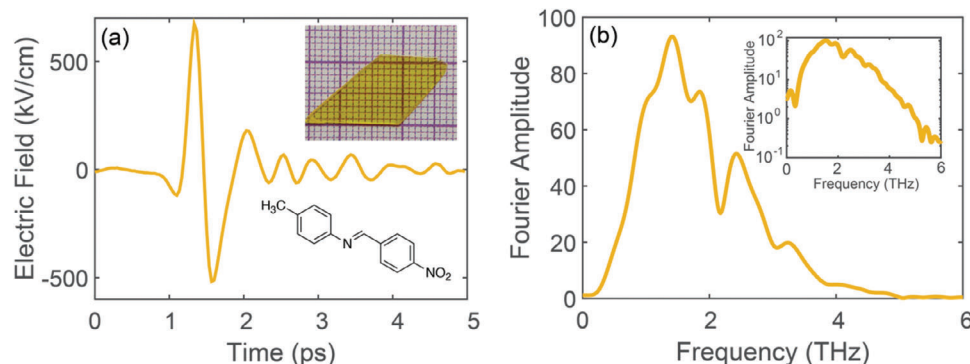
Figure 1. a) Time trace of NMBA at 1250 nm with insets showing an image of NMBA crystal and molecular structure of NMBA. b) Fourier transform of time trace in a) with inset showing the same data plotted using a logarithmic scale for the y-axis to emphasize broadness.

candidate for THz transmission measurements and other broadband THz applications.

2. Crystal Growth

2.1. Seed Growth

NMBA was synthesized as previously reported.[15] Thin fibers of NMBA were grown via a sublimation protocol in a thermally isolated 400 mL beaker, as shown in **Figure 2a**. In a typical procedure, 7 g of NMBA was added to the 400 mL beaker, which was then capped with insulation (cotton in aluminum foil) and immersed in a temperature-controlled sand bath, with the NMBA level in the flask below the level of the heated sand. The beaker was heated to 131 °C for 16 h, and then the temperature was cooled to 124 °C for 5 h. Maintaining the sublimation temperature at 124 °C allowed the NMBA vapor to slowly begin to condense and form fibers. After the 5 h period at 124 °C, the sand bath heater was turned off and the sample was cooled to room temperature. Finally, NMBA thin fibers (≈100–150 μm thick, 2–5 cm long) were harvested off the surface of the insulation (Figure 2b). This sublimation technique consistently produced about twenty 2–5 cm rectangular thin fibers of NMBA, as shown in Figure 2b. We attempted seed growth from various solvents but could not obtain seed crystals of sufficient quality to enable the growth of large windows of NMBA. The sublimation method, however, provided long, thin needles of NMBA that were sin-
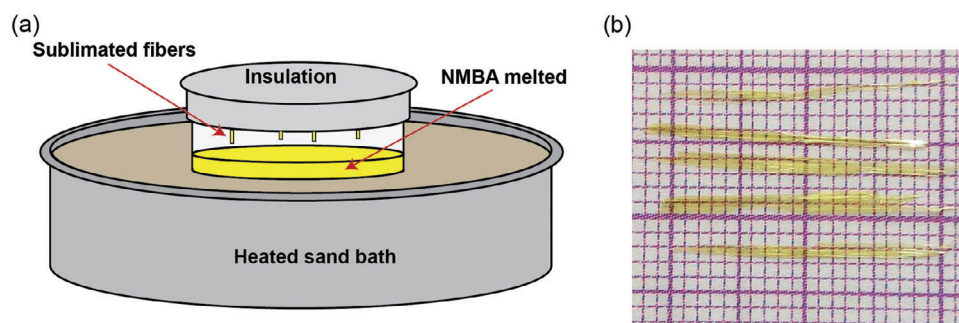
gle crystalline and suitable to be used as seeds for large crystal growth.
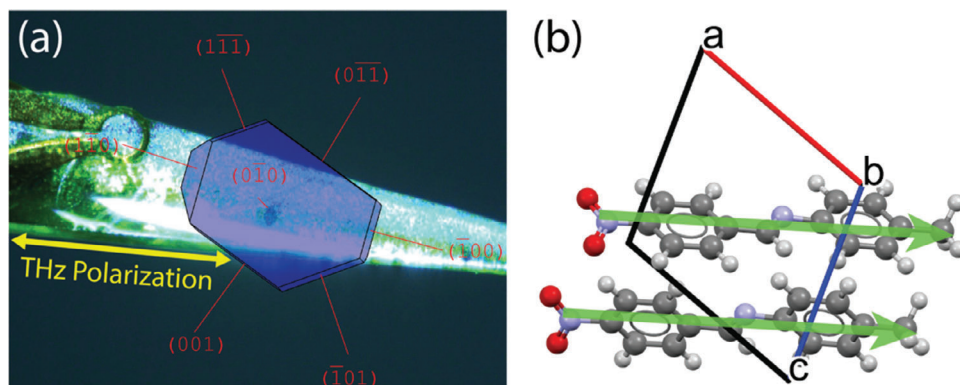
2.2. NMBA Crystal Growth

Large single-crystalline windows of NMBA were grown using the thin sublimed fibers as seed crystals. A supersaturated solution of NMBA (2.6 g NMBA in 50 mL of 7:1 Ethyl Acetate: Hexane) was filtered through a paper filter into a 150 mL flask and a single thin NMBA crystal from the sublimation growth process was added. The flask was then sealed with a rubber stopper and an 18-gauge needle was inserted through the stopper to allow for very slow evaporation of solvent. The solution was allowed to slowly evaporate for about seven days, or until the NMBA crystal reached the desired thickness. From 2.5 to 3 cm long sublimated seeds, this protocol was able to consistently facilitate formation of 4 mm × 4 mm to 7 mm × 7 mm crystals with thicknesses of about 1 mm. We also found that the longer NMBA seed crystals produced bigger NMBA crystals. The as-grown NMBA were polished using aluminum oxide polishing film (M9 grit followed by M3 grit) wet with ethanol to achieve the desired crystal thickness, followed by polishing on an ethanol-soaked microfiber cloth to refine the surface quality of the crystal.

2.3. X-Ray Crystal Structure

The structure of the grown NMBA crystals was confirmed with single-crystal X-ray diffraction (SC-XRD) (See section 2a in

Figure 2. a) Representation of crystallization method. b) Sublimated seed fibers.

**ADVANCED
SCIENCE NEWS**

www.advancedsciencenews.com

**ADVANCED
OPTICAL
MATERIALS**

www.advopticalmat.de

Figure 3. a) Face Index of a strip of NMBA crystal, showing the indexed cell in blue and the indexed crystallographic planes in red. The experimental THz polarization is indicated as the yellow arrow. b) A unit cell of NMBA, viewing along the b-axis. The hyperpolarizability vectors are indicated as the green arrows.

Supporting Information). The structure is consistent with the reported structure in the Cambridge Structure Database (CSD). An important factor of the THz generation ability of NLO crystals is the growth direction of the chromophores. The better the alignment of the polar axis of the crystal and the hyperpolarizability of the chromophores, the closer the order parameter is to 1. An order parameter of 1 corresponds to optimal chromophore alignment for maximum THz output. The order parameter of NMBA is 0.85. SC-XRD analysis also confirmed the main crystal face of the grown NMBA crystals as the (010) face, shown below in **Figure 3** (see section 2b in Supporting Information). Because these organic NLO crystals are birefringent, knowing the crystal face most aligned with the THz polarization axis is important in THz generation experiments.

3. Results

3.1. THz Generation Experiments

We characterized the THz generation properties of NMBA using the three parabolic mirror focusing systems described in our previous work.[16] The three-parabolic mirror system enables us to expand the THz beam to fill the final parabolic mirror that focuses the beam to a tight spot to generate high field strengths. We tested the THz generation from NMBA crystals using the 800 nm output of a Ti:sapphire laser with a pulse duration of 100 fs and a 500 Hz repetition rate. Because many of the NMBA crystals are mounted on 5 mm apertures, we used a telescope to reduce the $1/e^2$ beam diameter to $\approx$5.1 mm to ensure that nearly the full beam power interacted with the crystals. The beam has a typical pulse energy of $\approx$3.5 mJ per pulse, which we can vary with a $\lambda/2$ waveplate and polarizers.

We also pumped the NMBA crystals with longer wavelengths ranging from 1250–1550 nm, which were derived from the output of an optical parametric amplifier (OPA). These longer wavelengths have a pulse energy of $\approx$0.65 mJ per pulse and have a $1/e^2$ beam diameter of $\approx$7.6 mm. The THz generated with both 800 nm and longer wavelengths was measured using electro-optic (EO) sampling with an 800 nm, $\approx$100 fs variably delayed probe pulse. A 100-μm (110) GaP crystal bonded to a 1-mm (100) GaP crystal was placed at the focal point of the THz beam for EO

detection. The pulse duration of the setup limits the THz detection bandwidth to a maximum of $\approx$6 THz. High field strengths are sufficient to saturate our EO-detection scheme, so we used a pair of wire-grid polarizers to reduce the THz field strength. The field was attenuated by rotating the first polarizer and then scaled to its true magnitude corresponding to the expected field at a polarizer rotation of 0° (where there is maximum transmission through both polarizers).[17] The experiments were performed over several months on many NMBA crystals to ensure adequate crystal quality and field and spectral consistency (see Supporting Information).

The pump wavelength of 800 nm is particularly interesting due to the commercial availability of Ti: sapphire lasers. **Figure 4a** depicts a comparison of the UV-vis absorption cutoff for NMBA compared to BNA and MNA. We see NMBA has an absorption cutoff at $\approx$450 nm, BNA at $\approx$480 nm, and MNA at $\approx$500 nm (wavelengths at 25% transmission). NMBA absorbs much closer to 400 nm than the other two crystals. We hypothesize that the lower absorption cutoff in NMBA could enable it to be pumped efficiently at 1030 nm without any complications due to two-photon absorption, whereas there is likely some two-photon absorption with BNA and MNA. NMBA and MNA have a similar percent transmission of $\approx$67% at a wavelength of 800 nm, while the BNA percent transmission is at $\approx$80%. The sharp jump at 700 nm in the transmittance comes from a grating change in the UV-vis spectrometer. The inset of Figure 4a shows the measured 800-nm transmission through the crystals NMBA, BNA, and MNA as a function of fluence. Two-photon absorption is evident in all three crystals, because as the fluence increases, the percent transmission decreases for each of the crystals.

The laser-induced damage thresholds of BNA and NMBA are plotted in Figure 4b. The crystals damage due to a combination of their low melting points and two-photon absorption, which leads to heating the crystal above its melting point. The melting point of NMBA is higher than BNA (122 °C for NMBA vs 101 °C for BNA), which leads to an average damage threshold for NMBA (5.75 ± 0.43 mJ cm^{-2}) that is higher than that of BNA (4.43 ± 0.95 mJ cm^{-2}).

Figure 5 contains a comparison of the THz generation of NMBA, BNA, and MNA crystals (each $\approx$600 um thick) at 800 nm and 1250 nm pump wavelengths. The inorganic NLO crystal GaP
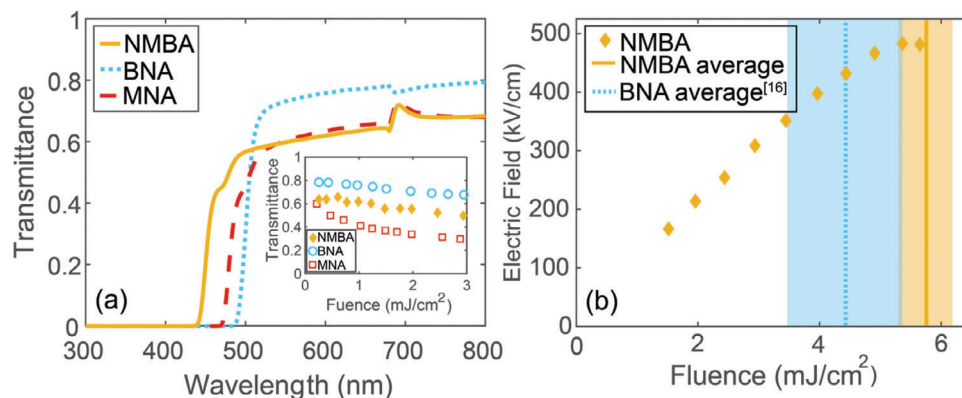
Figure 4. a) UV-vis transmittance from 300- to 800-nm for NMBA, BNA, and MNA. The inset shows the percent transmittance at 800-nm for the three crystals as a function of fluence. b) Plot of the electric field of NMBA as a function of fluence up until the point when the peak-to-peak electric field output begins to decrease due to damage. The solid and dotted lines indicate the average damage threshold of NMBA and BNA.[16] The boxes highlight the standard deviation in the damage threshold.
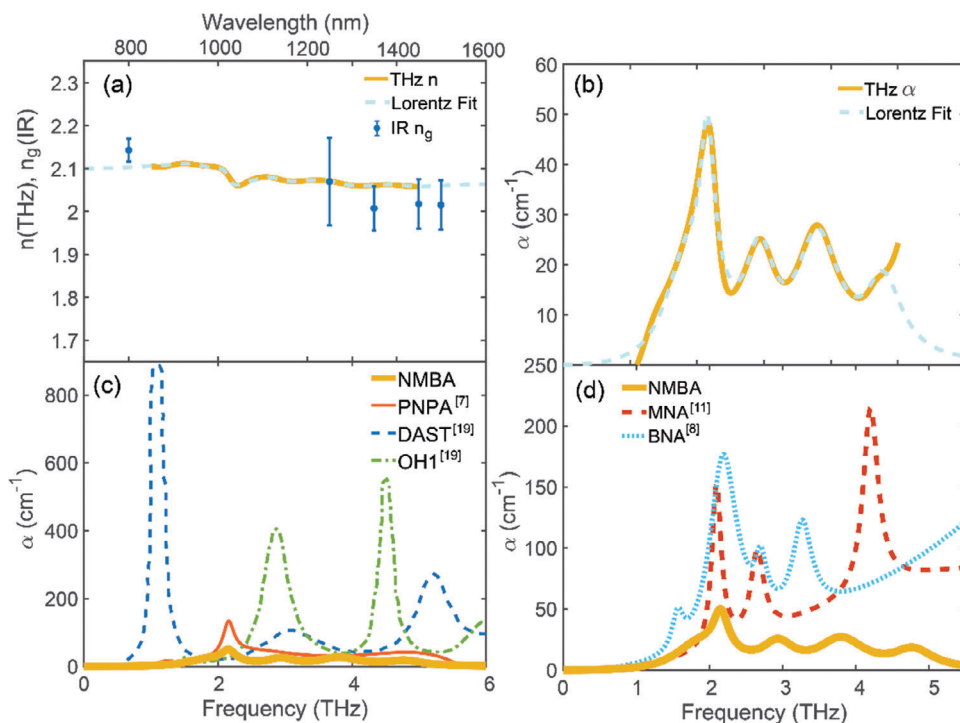
(300 um) is also included in the comparisons. Figure 5a depicts the time traces of generated THz pulses for each crystal pumped with 800-nm with a $1/e^2$ beam diameter of ≈0.51 cm and a pulse energy of ≈0.4 mJ per pulse (fluence of ≈1.95 mJ cm^{-2}). The associated spectra are included in Figure 5b. The BNA and MNA generate peak-to-peak field strengths of ≈400 kV cm^{-1} and NMBA has a peak-to-peak field strength of ≈200 kV cm^{-1}. The inset in

Figure 5b shows the THz generation efficiency for the three crystals. This was measured by comparing the power of the incoming IR light to the power of the generated THz measured with a pyroelectric detector. At 800 nm, and a maximum fluence of 1.9 mJ cm^{-2} (pulse energy of ≈0.4 mJ), BNA and MNA are more efficient THz generators reaching a maximum efficiency of ≈0.4%, while NMBA is lower with efficiency <0.1%.
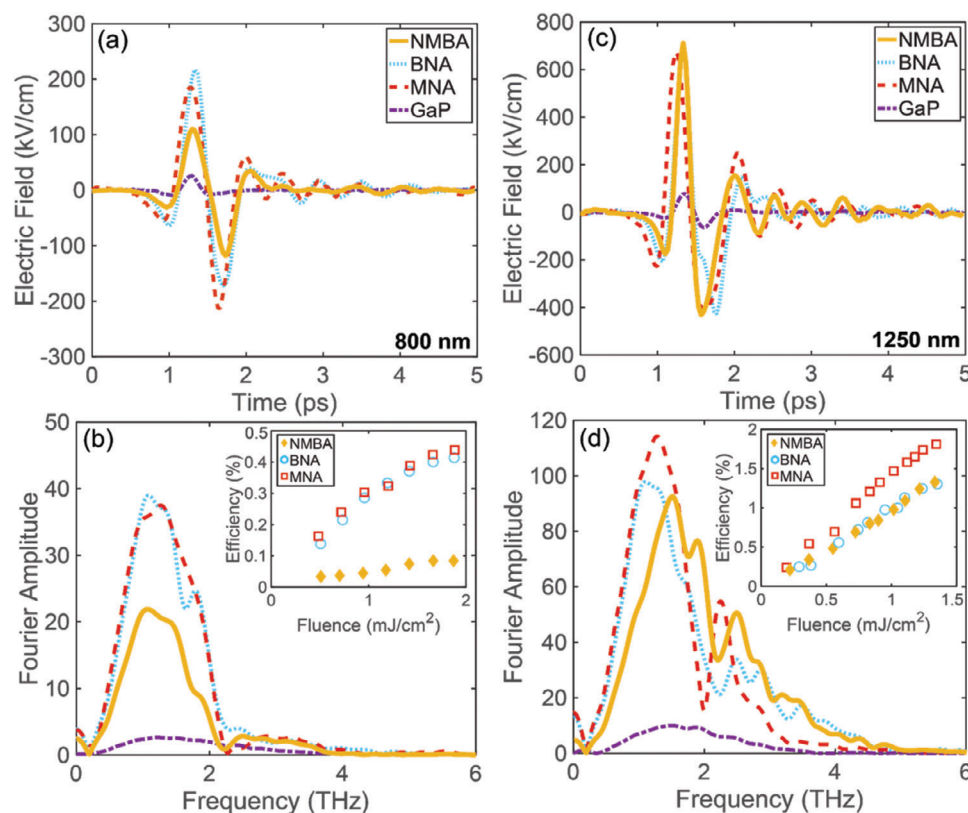
Figure 5. a) THz electric field traces for BNA, MNA, and NMBA at 800-nm pump wavelength. b) THz generation spectra at 800 nm with the inset showing the efficiency as a function of fluence. c) THz electric field traces at 1250-nm pump wavelength. d) THz generation spectra at 1250 nm with inset of the efficiency plot. For all subplots, NMBA is depicted with a solid yellow-orange line, BNA with a light blue dotted line, MNA with a red dashed line, and GaP with a purple dash-dotted line.

**ADVANCED
SCIENCE NEWS**

www.advancedsciencenews.com

**ADVANCED
OPTICAL
MATERIALS**

www.advopticalmat.de

Figure 6. a) Measured refractive index and Lorentz fit for NMBA with the IR group index shown at different wavelengths. The error bars are the standard deviation based on measurements taken of multiple crystals. b) Measured absorption coefficient and Lorentz fit for NMBA. c) Absorption coefficient comparison between NMBA and red THz generators PNPA, DAST, and OH1.[7,19] d) Absorption coefficient comparison between NMBA, BNA, and MNA.[8,11]

At 1250 nm pump wavelength (shown in Figure 5c,d), all three crystals are more efficient THz generators, because of better phase matching of longer IR wavelengths with generated THz frequencies. In these 1250-nm measurements, the crystals were pumped with ≈0.73 mJ pulses and a $1/e^2$ beam diameter of 0.76 mm. At these longer wavelengths, we observe smoother and broader spectra for all three crystals. The THz generation performance of NMBA is comparable to that of BNA and MNA, with all crystals showing peak-to-peak electric field strengths of ≈1 MV/cm. NMBA has an absorptive feature at ≈2 THz, similar to the other yellow crystals. We note that the absorption dip is weaker in NMBA than in BNA and MNA when pumped with 1250 nm light. All three crystals also show similar THz generation efficiencies at 1250 nm pump, with MNA slightly more efficient. The maximum fluence at 1.3 mJ cm^{-2} (pulse energy ≈0.6 mJ) corresponds to an efficiency of 1.8% for the MNA and 1.3% for the BNA and NMBA. The greater efficiency at longer wavelengths can be explained by better phase-matching (see below).
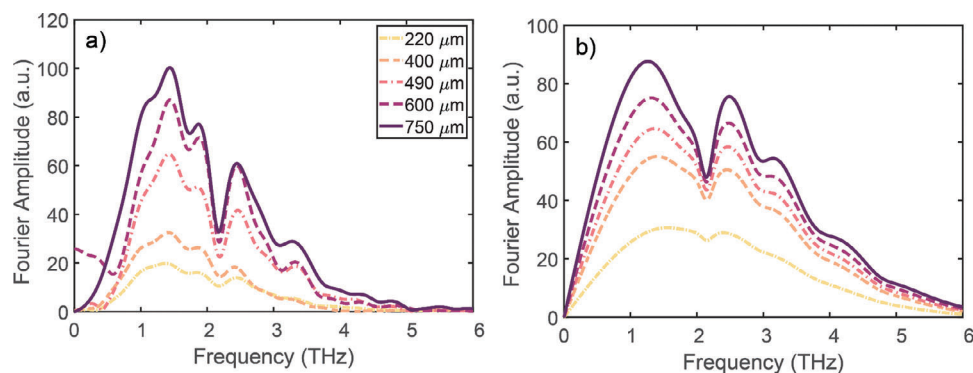
3.2. THz Phase Matching Properties

We performed THz transmission measurements on NMBA to extract the refractive index and absorption coefficient from 0 – 5 THz, and we fit the data shown using a Lorentz oscillator model. The Lorentz oscillator fit parameters are included in the supporting information. We also measured the IR group index at 800 nm and from 1250 to 1500 nm using an autocorrelator method.[18] The results are plotted in **Figure 6**a,b. The coherence length as a

function of pump wavelength is shown in Figure S5 (Supporting Information) in the supporting information. When the value of the group index at a particular wavelength overlaps with the refractive indices across the THz frequencies, the material is said to be well phase-matched. The group index at 800 nm (≈2.15) is less matched with the refractive index at frequencies >2 THz than the longer wavelengths. As such, we observe that when pumped with 1250 nm light, the NMBA spectrum has more amplitude at these higher frequencies. This contributes to a higher overall THz conversion efficiency for these longer wavelengths.

The THz absorption coefficient of NMBA reaches a maximum value of approximately 50 cm^{-1} at 2 THz, making it a THz generating material with one of the lowest maximum absorption coefficients in the range below 6 THz.[19] For example, BNA and MNA have maximum absorption coefficients in excess of 150 cm^{-1}.[8,11] DAST has very strong absorptions at 1 and 5 THz.[20] Other red crystals such as PNPA and OH1 also have stronger absorptions than NMBA.[7,20] This is what gives NMBA its broad spectrum with minimal absorption dips, making it an excellent THz generator for this range of frequencies. A comparison of these absorption coefficients is shown in Figure 6c,d.

A smooth, broad spectrum is ideal for field-resolved THz transmission measurements, which convey information about the material thickness, absorption coefficient, refractive index, and other material parameters. Strong absorptions block out information at certain frequencies. Because NMBA does not have strong THz absorptions, it is a great candidate for these measurements.

Finally, we modeled the THz spectrum of NMBA using the THz and optical parameters we extracted from our

**ADVANCED
SCIENCE NEWS**

www.advancedsciencenews.com

**ADVANCED
OPTICAL
MATERIALS**

www.advopticalmat.de

Figure 7. a) Thickness dependence of NMBA for crystal thicknesses ranging from 220 to 750 microns at a pump wavelength of 1250 nm. b) Modeled THz generation spectra for the same range of thicknesses using optical pump parameters at 1250 nm.

measurements. We used a group index of 2.06, which corresponds to the group index at a pump wavelength of 1250 nm. **Figure 7** shows a comparison of the modeled spectrum with experimental results for a range of NMBA crystal thicknesses. We note that THz output scales with crystal thickness. With most other THz generation crystals, thicker crystals can generate weaker pulses due to stronger absorptions. Additionally, because the step in the refractive index is smaller for NMBA than other materials, there is better phase matching across the range of generated THz frequencies, resulting in less destructive interference at higher frequencies that typically worsens with increased thickness.

4. Conclusion

From our previously reported data mining studies, the yellow organic NLO crystal NMBA was identified as a promising THz generation source. Here we optimized the crystal growth procedure of NMBA and obtained high-quality crystals through a two-step growth process. We characterized the THz generation properties of NMBA and compared it to other yellow organic NLO crystals BNA and MNA. NMBA is comparable to these yellow crystals when pumped with longer wavelengths, and at 1250 nm has a peak-to-peak electric field of 1 MV cm^{-1}. Unlike red organic NLO crystals, NMBA can be pumped with shorter wavelengths like 800 nm without significant damage from 2-photon absorption. This allows for the use of pump sources like Ti: sapphire lasers (800 nm) and Yb-doped lasers (1030 nm). With an absorption coefficient of <50 cm^{-1} over the 0–6 THz range and good phase matching especially at a pump wavelength of 1250 nm, NMBA generates a smooth, broad THz generation spectrum making it an ideal candidate for THz transmission measurements.

Supporting Information

Supporting Information is available from the Wiley Online Library or from the author.

Acknowledgements

Conflict of Interest

The authors declare no conflict of interest.

Data Availability Statement

The data that support the findings of this study are available from the corresponding author upon reasonable request.

Keywords

[1] B.-R. Shin, I. C. Yu, M.-H. Shin, M. Jazbinsek, F. Rotermund, O. P. Kwon, *APL Mater.* **2023**, *11*, 011101.

[2] F. D. J. Brunner, O. P. Kwon, S.-J. Kwon, M. Jazbinšek, A. Schneider, P. Günter, *Opt. Express* **2008**, *16*, 16496.

[3] S. R. Marder, J. W. Perry, W. P. Schaefer, *Science* **1989**, *245*, 626.

[4] S. R. Marder, J. W. Perry, C. P. Yakymyshyn, *Chem. Mater.* **1994**, *6*, 1137.

[5] B. Monoszlai, C. Vicario, M. Jazbinsek, C. P. Hauri, *Opt. Lett.* **2013**, *38*, 5106.

[6] A. Schneider, M. Neis, M. Stillhart, B. Ruiz, R. U. A. Khan, P. Günter, *J. Opt. Soc. Am. B* **2006**, *23*, 1822.

[7] C. Rader, Z. B. Zaccardi, S.-H. E. Ho, K. G. Harrell, P. K. Petersen, M. F. Nielson, H. Stephan, N. K. Green, D. J. H. Ludlow, M. J. Lutz, S. J. Smith, D. J. Michaelis, J. A. Johnson, *ACS Photonics* **2022**, *9*, 3720.

[8] I. C. Tangen, G. A. Valdivia-Berroeta, L. K. Heki, Z. B. Zaccardi, E. W. Jackson, C. B. Bahr, S.-H. Ho, D. J. Michaelis, J. A. Johnson, *J. Opt. Soc. Am. B* **2021**, *38*, 2780.

[9] M. Shalaby, C. Vicario, K. Thirupugalmani, S. Brahadeeswaran, C. P. Hauri, *Opt. Lett.* **2016**, *41*, 1777.

[10] H. Zhao, Y. Tan, T. Wu, G. Steinfeld, Y. Zhang, C. Zhang, L. Zhang, M. Shalaby, *Appl. Phys. Lett.* **2019**, *114*, 241101.

[11] B. W. H. Palmer, C. Rader, E. S.-H. Ho, Z. B. Zaccardi, D. J. Ludlow, N. K. Green, M. J. Lutz, A. Alejandro, M. F. Nielson, G. A. Valdivia-

**ADVANCED
SCIENCE NEWS**

www.advancedsciencenews.com

**ADVANCED
OPTICAL
MATERIALS**

www.advopticalmat.de

Berroeta, C. C. Chartrand, K. M. Holland, S. J. Smith, J. A. Johnson, D. J. Michaelis, *ACS Appl. Electron. Mater.* **2022**, *4*, 4316.

[12] M. Savoini, L. Huber, H. Cuppen, E. Abreu, M. Kubli, M. J. Neugebauer, Y. Duan, P. Beaud, J. Xu, T. Rasing, S. L. Johnson, *ACS Photonics* **2018**, *5*, 671.

[13] C.-U. Jeong, B. Kang, S.-H. Lee, S.-C. Lee, W. Kim, M. Jazbinsek, W. Yoon, H. Yun, D. Kim, F. Rotermund, O. P. Kwon, *Adv. Funct. Mater.* **2018**, *28*, 1801143.

[14] G. A. Valdivia-Berroeta, Z. B. Zaccardi, S. K. F. Pettit, S.-H. Ho, B. W. Palmer, M. J. Lutz, C. Rader, B. P. Hunter, N. K. Green, C. Barlow, C. Z. Wayment, D. J. Ludlow, P. Petersen, S. J. Smith, D. J. Michaelis, J. A. Johnson, *Adv. Mater.* **2022**, *34*, 2107900.

[15] K. Srinivasan, R. Biravaganesh, R. Gandhimathi, P. Ramasamy, *J. Cryst. Growth* **2002**, *236*, 381.

[16] Z. B. Zaccardi, I. C. Tangen, G. A. Valdivia-Berroeta, C. B. Bahr, K. C. Kenney, C. Rader, M. J. Lutz, B. P. Hunter, D. J. Michaelis, J. A. Johnson, *Opt. Express* **2021**, *29*, 38084.

[17] C. Rader, M. F. Nielson, B. E. Knighton, Z. B. Zaccardi, D. J. Michaelis, J. A. Johnson, *Opt. Lett.* **2022**, *47*, 5985.

[18] L. Mutter, F. D. Brunner, Z. Yang, M. Jazbinšek, P. Günter, *J. Opt. Soc. Am. B* **2007**, *24*, 2556.

[19] J. Lu, S.-H. Lee, X. Li, S.-C. Lee, J.-H. Han, O. P. Kwon, K. A. Nelson, *Opt. Express* **2018**, *26*, 30786.

[20] M. Jazbinsek, U. Puc, A. Abina, A. Zidansek, *Appl. Sci.* **2019**, *9*, 882.